Asian Journal of Chemistry; Vol. 37, No. 11 (2025), 2759-2765
ASIAN JOURNAL OF CHEMISTRY
https://doi.org/10.14233/ajchem.2025.34345

Thermal and Electrochemical Studies of PANI-Graphene Nanocomposite on Mild Steel in Acidic Media

KARTHIKA SHETTY[1], JAYADEV[2] and ARJUN SUNIL RAO[3,*]

[1]Department of Chemistry, R.N.S. Institute of Technology, Bangalore-560098, India
[2]Department of Chemistry, S.J.B. Institute of Technology, Bangalore-560060, India
[3]Department of Electronics and Communication Engineering, Manipal Institute of Technology, Manipal Academy of Higher Education (MAHE), Manipal, Udupi-576104, India

*Corresponding author: E-mail: arjun.rao@manipal.edu

Received: 26 June 2025 *Accepted*: 22 September 2025 *Published online*: 27 October 2025 AJC-22164

In present study, Epoxy-coated polyaniline-graphene nanocomposites (PGNCs) were synthesized *via in situ* polymerization to investigate their thermal stability and electrochemical performance as protective coatings on mild steel in acidic environments. The PGNCs were characterized using Fourier-transform infrared spectroscopy (FT-IR), thermogravimetric analysis (TGA), scanning electron microscopy (SEM), ultraviolet-visible spectroscopy (UV-Vis), Raman spectroscopy and X-ray diffraction (XRD). To evaluate their anticorrosive performance, the synthesized PGNCs were incorporated into an epoxy matrix composed of araldite resin and a hardener. Various concentrations of PGNC were uniformly dispersed in a fixed volume of the epoxy system using a mechanical mixing method. The resulting epoxy nanocomposite coatings were then applied onto mild steel substrates and exposed to acidic media. Corrosion protection efficiency was assessed using electrochemical measurements performed with an electrochemical workstation.

Keywords: Polyaniline, Conducting polymer, Graphene, Polymerization, Corrosion studies.

INTRODUCTION

Graphene, a two-dimensional allotrope of carbon, exhibits exceptional physical and chemical properties that distinguish it from other carbon allotropes. It possesses a theoretical surface area of 2630 m^2/g and a specific capacitance of 550 F/g [1]. With mechanical strength approximately 100 times greater than steel, graphene has an elastic modulus of ~1 TPa and tensile strength near 100 GPa, making it one of the hardest and strongest known materials. Its remarkable thermal conductivity, transparency and flexibility as a conductor contribute to its wide range of applications in solar cells, LEDs, touch panels and smartphones. Despite these advantages, structural defects and interlayer van der Waals forces often lead to agglomeration, limiting performance in some applications [2].

All carbon atoms in graphene are sp^2-hybridized, which contributes to its unique electronic, thermal and mechanical behaviour [3]. Graphene is chemically stable at room temperature and exhibits nonlinear diamagnetism. Its excellent solubility, especially in modified forms like graphene oxide (GO), allows it to be used in a variety of hybrid nanocomposite systems [4]. A growing body of research has focused on the corrosion-resistant properties of conductive graphene materials.

Polyaniline (PANI), an intrinsically conductive polymer (ICP), has also attracted significant attention due to its structural flexibility, tuneable electrical properties, environmental stability and high electrochemical activity [4]. The photoconductivity, reversible doping behaviour and ease of synthesis of PANI from inexpensive monomers make it attractive for a variety of applications, including sensors, antistatic coatings, corrosion resistance and electrochromic displays [5]. Studies have demonstrated that combining PANI with metal oxides or incorporating it into nanocomposites can enhance corrosion protection compared to PANI alone [5,6].

Among various methods for synthesizing polymer nanocomposites such as solution mixing, melt blending and *in situ* polymerization the *in situ* approach is most widely used for fabricating graphene-based nanocomposites (PGNC). In current study, PGNCs were synthesized *via in situ* polymerization using ammonium persulfate (APS) as oxidizing agent. This method

promotes covalent cross-linking and also facilitates non-covalent interactions in polymer matrices such as polyethylene, polyacrylics and polypyrroles [7].

For corrosion protection, epoxy-based coatings were employed due to their strong adhesion, mechanical durability, chemical resistance and cost-effectiveness [8]. In this work, an epoxy resin (araldite) was used to form a protective coating over mild steel substrates. Despite their advantages, epoxies have limitations, including brittleness, low crack resistance and hydrophilic hydroxyl groups that increase permeability to water, oxygen and chloride ions, all of which can accelerate substrate corrosion over time [9]. Moreover, mild steel structures are highly susceptible to corrosion, particularly in acidic environments used in industrial applications such as acid cleaning, pickling and well acidification. Organic corrosion inhibitors containing nitrogen, sulphur or oxygen are often used to reduce the dissolution rate of metal surfaces. These inhibitors function primarily through adsorption on the metal surface, forming a protective barrier. The ideal inhibitor is characterized by high efficiency, low toxicity, affordability and ease of production [10].

In this study, we aimed to optimize the synthesis parameters of prepared PGNCs and evaluate their anti-corrosion performance when applied as coatings on the mild steel. The protective behaviour of the coatings was investigated using electrochemical techniques in acidic environments. The results highlight the effectiveness of graphene-based epoxy composites in enhancing the corrosion resistance and provide insight into their potential for scalable applications in aggressive chemical environments.

EXPERIMENTAL

Polyaniline (PANI), ammonium persulphate (APS) and hydrochloric acid were purchased from SD Fine-Chem Ltd., India and used without further purification. Graphene was obtained from Sigma-Aldrich, USA for synthesis. Araldite epoxy resin (Huntsman, USA) served as polymer matrix, while AISI 316 stainless steel substrates were employed for the coating and electrochemical evaluations. The steel test material (ASTM A 240/A240M-16) with a chemical composition, 0.22%C, 0.041%P, 0.003%S, 1.22% Mn, 0.41% Si was used.

Synthesis of nanostructured PANI-graphene nanocomposites (PGNC): Graphene was dispersed in HCl under sonication and mixed with 5 mL of pre-distilled aniline with constant stirring for 20 min. The mixture was reacted for 10 h, followed by the addition of 5 g of APS dissolved in 25 mL deionized water as oxidant. Polymerization was continued for another 10 h and then left overnight. The resulting product was filtered using HCl, acetone and deionized water, then dried in an oven for 15 h to obtain a dry green PANI-graphene nanocomposite.

Instrumentation: The molecular structure of crystals was analyzed by using XRD (D8ADVANCE ECO Bruker; 1KW Cu*K*α λ = 1.54 Å). Surface image of the synthesized sample can record by using SEM (HITACHI SU3500N to variable voltage 30 k V). Infra spectrum of absorption was measured using FT-IR (Shimadzu IR Affinity-ISWL of wave number 350-7800 cm^{-1}). Weight loss measurement was performed (Shimadzu DTG-60RT, max 1000 ºC) in nitrogen atmosphere), the absorptive measurements was performed by using UV-visible spectrometry (Shimadzu UV 2600), Raman shift measured by using Lab Ram HR Spectrometer, whereas corrosion study was performed using the electrochemical workstation [11].

RESULTS AND DISCUSSION

Surface morphology: The surface morphology, structure and graphene coating of the synthesized composites were studied using scanning electron microscopy (SEM) technique. The SEM image of mild steel immersed in 0.25 M HCl (Fig. 1a) displays an amorphous surface with significant agglomeration [11], whereas pure graphene (Fig. 1b) exhibits a distinct flake like structure, consistent with its layered morphology [12]. The SEM image of the PANI-graphene nanocomposite (PGNC) (Fig. 1c) reveals a well-interlocked structure, indicating successful incorporation of polyaniline within the graphene matrix. The morphological changes observed in PGNC are attributed to the uniform assemblage of PANI on the graphene surface, confirming the effective synthesis and enhanced dispersion of PANI, which contributes to the structural integrity of the composite.

FT-IR spectral studies: The FT-IR spectra of the PANI-graphene nanocomposite (PGNC) are shown in Fig. 2. For graphene, characteristic peaks appear at 499 cm^{-1} and 3410 cm^{-1}, corresponding to O–H stretching vibrations. A peak at 3451 cm^{-1} is attributed to tensile vibrations of –OH groups,

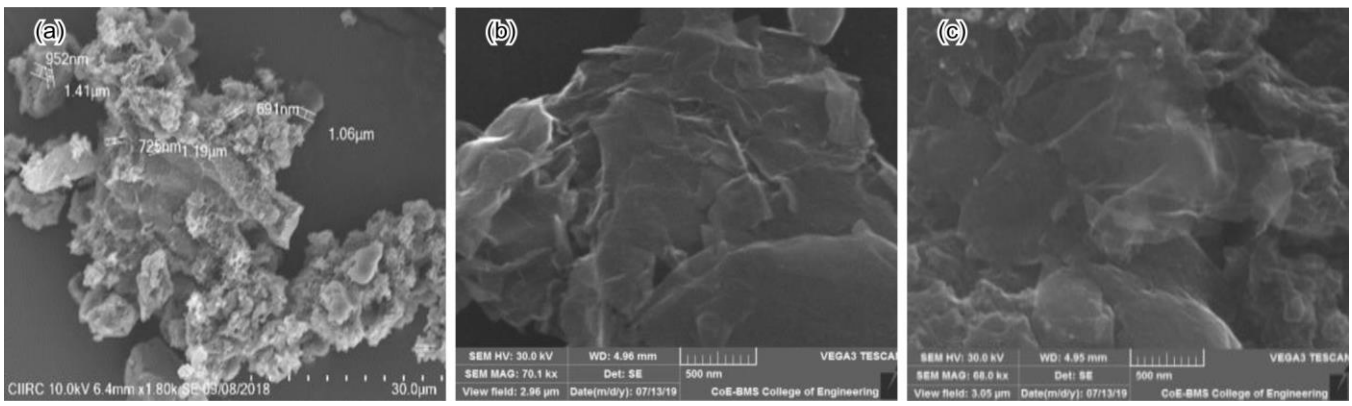

Fig. 1. SEM images of (a) PANI, (b) graphene and (c) PGNC

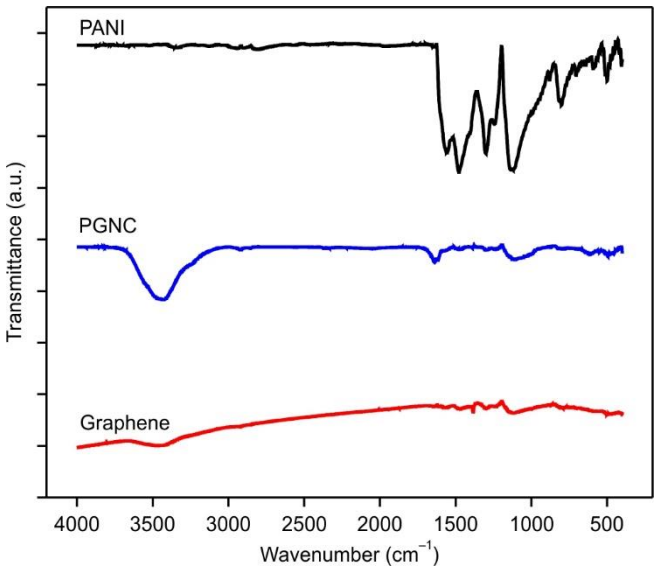

Fig. 2. FT-IR spectra of PANI, graphene and PGNC

while the peak at 1614 cm^{-1} is due to the C=O stretching in carboxylic acid (COOH) groups. Moreover, the C–O–C and –OH vibrations contribute to peaks at 1383 cm^{-1} and 1110 cm^{-1}, respectively.

Pure polyaniline (PANI) exhibits peaks at 787 cm^{-1} and 1295 cm^{-1}, assigned to out-of-plane bending of C–H and in-plane bending of C–N stretching in the benzenoid ring (N=Q=N) [13-15]. Consistent with previous reports, peaks near 788 cm^{-1} correspond to N–H out-of-plane bending, 857 cm^{-1} to *para*-disubstituted aromatic rings and 1292 cm^{-1} to C–N stretching vibrations. The unsymmetrical C6 ring stretching mode is represented by two bands at 1453 cm^{-1} and 1614 cm^{-1}, corresponding to C=C stretching in benzenoid and quinoid rings, respectively. The quinoid ring predominantly contributes to the higher frequency band, while the benzenoid ring influences the lower frequency band.

In the PGNC composite, a peak at 855 cm^{-1} is attributed to C–C bending vibrations. The vibrations of –OH and C–O–C groups generate peaks around 1080 cm^{-1} and 1110 cm^{-1}, respectively [16]. These spectral features confirm the successful incorporation of graphene within the PANI matrix, consistent with previous studies (Table-1). Thus, FT-IR analysis effectively validates the presence of graphene in the composite structure.

TABLE-1
KEY FT-IR ABSORPTION PEAKS OF PANI, GRAPHENE AND PGNC

Vibrational assignment	PANI (ν_{max}, cm^{-1})	Graphene (ν_{max}, cm^{-1})	PGNC (ν_{max}, cm^{-1})
C-O stretching		1110	1080
N=Q=N stretching	1453	–	1614
N-B-N stretching	1292	–	1383
C-OH stretching	1130	–	1292
C-O-C out of plane		1393	1090
-OH stretching	3301	3442	3432

Thermal studies: The thermal stability of the PANI-graphene nanocomposite (PGNC) was investigated using thermogravimetric analysis under a nitrogen atmosphere (Fig. 3). The TGA curve for PGNC (Fig. 3c) reveals three distinct stages of weight loss. The first stage occurs between approximately 24 ºC and 195 ºC, with a 10% mass loss attributed to the evaporation of physically adsorbed water. The second stage, ranging from 195 ºC to 322 ºC, shows a 4% weight loss caused by the degradation of C–O bonds and other oxygen-containing functional groups. The third and most significant stage of decomposition occurs between 322 ºC and 800 ºC, accounting for a 73% mass loss, which is likely due to the removal of more stable oxygen-containing groups and the breakdown of the graphene structure.

For pure polyaniline (PANI), the TGA curve (Fig. 3b) similarly shows three weight loss stages. The first stage, from 20 ºC to 70 ºC, corresponds to the vaporization of any unreacted monomer. The second stage, between 70 ºC and 282 ºC, is related to the decomposition of hydrochloric acid dopants in the polymer. The third stage, extending from 282 ºC to 700 ºC, represents the degradation of the polymer backbone. The PGNC composite (Fig. 3d) exhibits a similar degradation pattern to PANI but demonstrates improved thermal stability overall (Table-2). This enhanced stability is attributed to the incorporation of graphene, which reinforces the composite structure and slows the degradation process compared to pure PANI.

TABLE-2
WEIGHT LOSS MEASUREMENTS OF THERMOGRAMS

PGNC (w/w%)	Process	Transition temperature range ± 2 ºC			Weight loss (%)
		T_i	T_{max}	T_c	
PANI	1	20	41	70	6
	2	70	184	282	15
	3	282	447	700	78
	Residue				1
PGNC	1	24	128	195	10
	2	195	247	322	4
	3	322	544	800	73
	Residue				13
Graphene	1	30	139	214	1
	2	214	238	791	2
	Residue				97

X-ray diffraction: Fig. 4 presents the X-ray diffraction (XRD) patterns of pure polyaniline (PANI) and the PGNC. The pure PANI exhibits a broad diffraction band around 2θ = 25º, indicative of its amorphous nature [17,18]. In contrast, the PGNC displays a sharp, intense peak at 2θ = 26.6º, along with several other peaks at 37.39º, 45.95º, 54.5º and 77.9º, corresponding to the (200), (020) and (011) crystal planes, respectively. These distinct peaks confirm the crystalline nature of the graphene component within the composite. The comparison of the XRD patterns suggests that PANI has been successfully deposited onto the graphene surface, resulting in the formation of the nanocomposite with enhanced structural ordering.

Raman spectral studies: Raman spectra of the PANI-PGNC exhibit the characteristic peaks (Fig. 5) that confirm its structural features. A prominent peak at 1358 cm^{-1}, known as the D band, corresponds to nanocrystalline defects and arises from out-of-plane vibrations in the graphene structure. The G

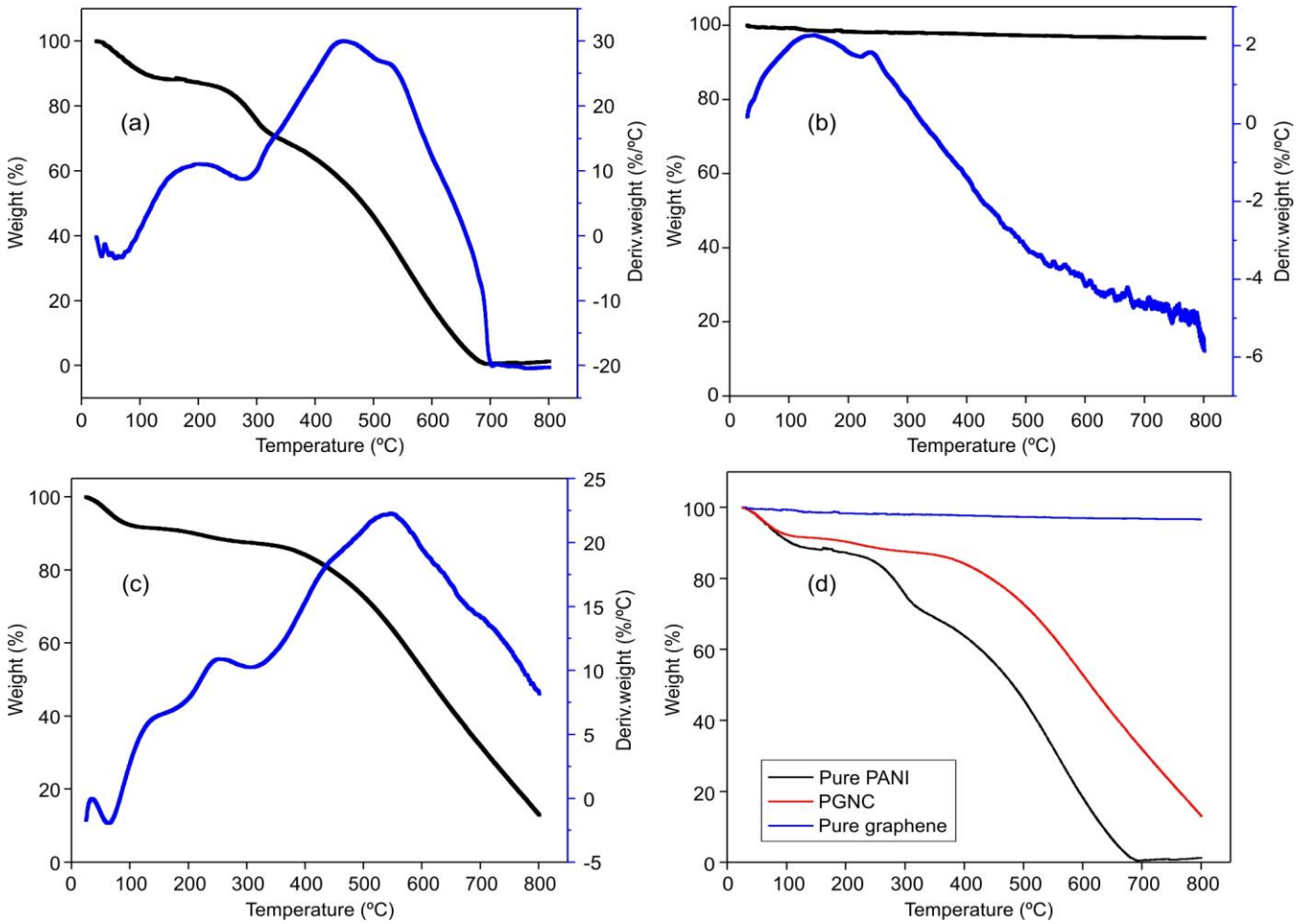

Fig. 3. Derivative thermograms of (a) PANI, (b) graphene, (c) PGNC and (d) combined a, b, c

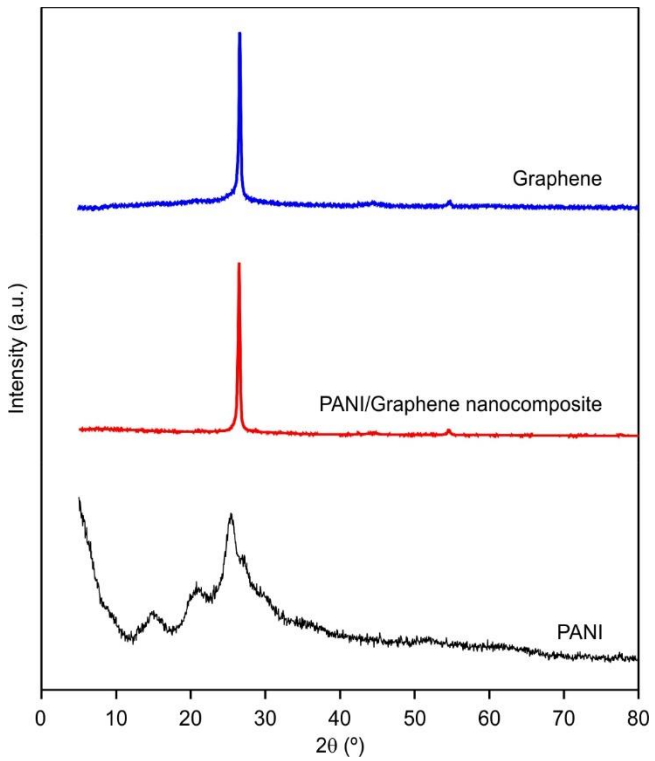

Fig. 4. XRD pattern of PANI, graphene and PGNC

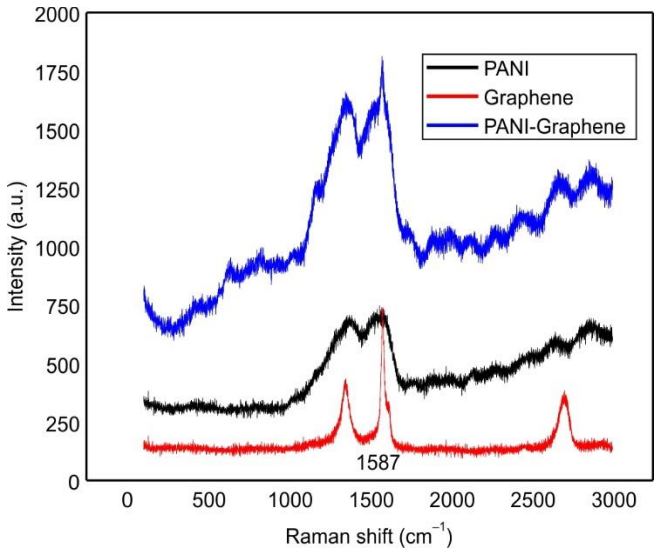

Fig. 5. Raman spectra of PANI, graphene and PGNC

band appears at 1587 cm^{-1} and is attributed to the E_{2g} mode of sp^2-hybridized carbon atoms, representing the in-plane vibrations of the graphene lattice. Furthermore, a strong G* band is observed at 2704 cm^{-1}, corresponding to in-plane vibrational modes of sp^2 carbon, which show significant dependence on the laser excitation energy. These peaks collectively confirm

the presence of graphene with both crystalline and amorphous carbon characteristics in the PGNC composite.

UV-visible studies: Fig. 6 shows the UV-visible absorption spectra of PANI, graphene and the PANI-graphene nanocomposite (PGNC) dispersed in DMF. Graphene exhibits a sharp peak at 273 nm, attributed to the π–π* electronic transition, along with a shoulder peak at 295 nm associated with n–π* transitions caused by oxygen-containing functional groups such as epoxy, hydroxyl and carboxyl groups. PANI shows characteristic absorption peaks at 341 nm, corresponding to the π–π* transition of the benzenoid ring and at around 426 nm due to quinoid excitation. The PGNC spectrum contains absorption peaks at 341 nm and 426 nm, similar to pure PANI, along with a distinct graphene peak at 270 nm. The incorporation of graphene into the PANI matrix enhances π–π* interactions between the composite components, leading to a decrease in the energy gap (ΔE). This is evidenced by the observed red shift in the absorption peaks, confirming strong interactions between PANI and graphene within the composite. These findings are consistent with the FT-IR and Raman spectroscopy results.

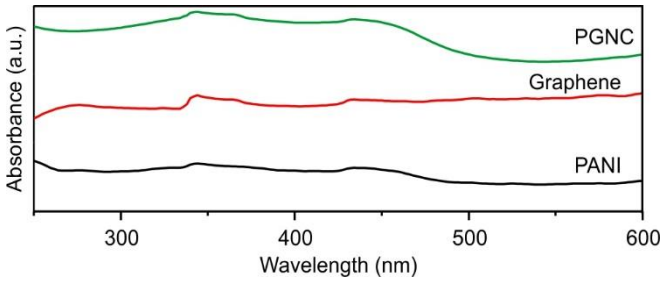

Fig. 6. Visible spectra of PANI, graphene and PGNC

Corrosion analysis

Synthesis of PGNC-epoxy coating: The synthesis of the PGNC-epoxy coating involves two main steps:

(i) Surface preparation of steel for coating: The mild steel substrate was cut into dimensions of 2 cm × 1 cm. The surface was degreased using dilute sulfuric acid to remove rust and other contaminants. Subsequently, the substrates were sonicated to eliminate residual impurities. After drying with a dryer, the surface was further cleaned with acetone and rinsed thoroughly with demineralized water. Finally, the prepared substrates were dried in an oven at 40 ºC to ensure complete removal of moisture.

(ii) PGNC-epoxy nanocomposite preparation and coating: PGNC powders were weighed in varying weight percentages (0.002%, 0.004%, 0.006%, 0.008% and 0.01%) with a thickness of approximately 0.321 nm and mixed uniformly with a fixed amount of epoxy resin. The resulting PGNC-epoxy mixture was mechanically applied onto the cleaned steel substrates. The coated samples were then dried in an oven at 50 ºC to cure the coating. Corrosion resistance of the coated steel was evaluated using potentiodynamic polarization measurements [19].

Corrosion protection mechanism of PGNC on mild steel: The PGNC coating was applied to mild steel *via* chemical oxidative polymerization of PANI with functionalized graphene in a 0.25 M HCl solution, using $(NH_4)_2S_2O_8$ as the oxidizing agent. This process resulted in well-dispersed graphene within the PANI matrix [19]. The corrosion mechanism on the coated steel involves oxidation of Fe at the anodic sites (working electrode), releasing electrons. These electrons participate in reduction reactions at the cathodic sites. The PGNC coating acts as a barrier, reducing the corrosion rate by hindering the electrochemical reactions on the steel surface. The reaction as follows:

At cathode:

$$2H_2O + 2e^- \rightarrow H_2 + 2OH^-$$

$$Fe^{2+} + 2OH^- \rightarrow Fe(OH)_2$$

$$4Fe(OH)_2 + 2H_2O + O_2 \rightarrow 2(Fe_2O_3 \cdot 3H_2O)$$

At anode:

$$Fe \rightarrow Fe^{2+} + 2e^-$$

At cathode, reduction of oxygen occurs by consuming electrons from anodic end, so that ferrous hydroxides are formed. In an excessive corrosive environment rust develops. The addition of PGNC inhibits the oxidation reaction, avoids the contact of Fe^{3+} ions, thus preventing the corrosion of the steel.

Potentiodynamic polarization studies: The electrochemical corrosion measurements were carried out using a three-electrode setup, where the PGNC-coated mild steel (MS) substrate served as the working electrode, Ag/AgCl as the reference electrode and platinum as the counter electrode. The potentiodynamic polarization curves for mild steel coated with graphene-doped epoxy and unreinforced epoxy in 0.25 M HCl solution are summarized in Table-3. These results include corrosion current density (i_{corr}), corrosion potential (E_{corr}), Tafel slopes and corrosion rates. The corrosion behaviour of mild steel was evaluated electrochemically by extrapolating the linear portions of the anodic and cathodic Tafel regions to determine the i_{corr} and E_{corr} values.

The bare steel exhibited an i_{corr} of 3.957×10^{-4} A. After coating with PGNC epoxy, i_{corr} decreased significantly to values less than 1.847×10^{-4} A and 3.575×10^{-5} A, indicating enhanced corrosion inhibition [19]. The graphene-containing coating, combined with araldite as a binder, effectively reduces corrosion due to its inhibitory nature. Correspondingly, the E_{corr} values shifted from -1.02 V for bare steel to -0.97 V and -0.84 V for epoxy-coated and PGNC-coated steel, respectively

TABLE-3
TAFEL PARAMETER PGNC IN 0.25 M HCl SOLUTION

Concentration of PGNC (ppm)	Dc (1/V)	Da (1/V)	E_{corr} (V)	R (Ω)	Corrosion I (A)
Blank	3.485	3.339	-1.1010	69	3.957e-004
50	4.231	3.722	-0.9849	243	1.305e-004
100	3.835	3.897	-0.9670	248	1.847e-004
150	4.100	4.786	-0.9543	840	3.575e-005

(Fig. 7) [20]. The positive shift in E_{corr} alongside the substantial reduction in i_{corr} confirms that PGNC coatings provide superior corrosion resistance in acidic environments.

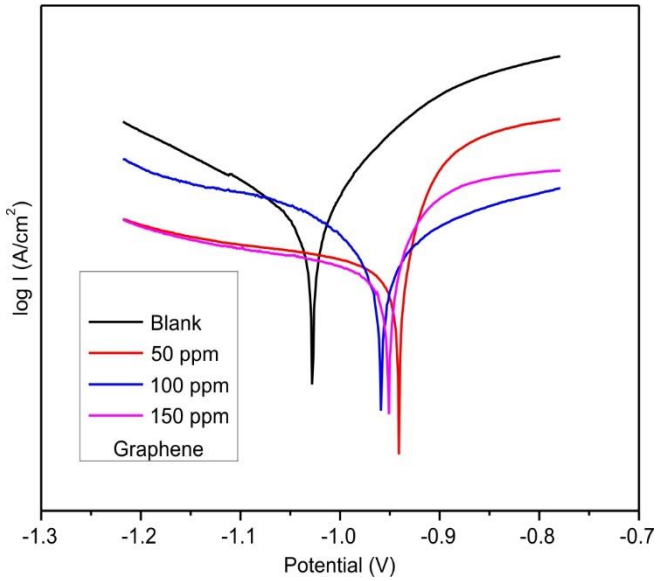

Fig. 7. Tafel plot PANI reinforce graphene

Open circuit potential (OCP) and electrochemical impedance spectroscopy (EIS) analysis: The OCP measurements reveal a significant shift from -1.218 V for bare steel to -0.778 V for the PGNC-coated steel, indicating that PGNC acts as an effective corrosion inhibitor. As the PGNC concentration increases, the corrosion rate correspondingly decreases, as clearly shown in Fig. 8a. The electrochemical parameters derived from the Tafel curves are summarized in Table-3.

Fig. 8b presents the Nyquist plots for steel coated with PGNC. The large semicircle observed corresponds to the coating's barrier strength, while the smaller semicircle relates to the steel substrate beneath the coating [21-24]. The semicircles appearing in the high-frequency region indicate the charge transfer resistance at the interface between the coating and the steel surface. A larger semicircle diameter signifies higher charge transfer resistance and thus lower electrode conductivity, demonstrating better corrosion protection [25,26].

Morphological studies: Fig. 9a shows the severe corrosion damage on the uncoated mild steel sample, highlighting the aggressive effect of the corrosive environment. At a lower PGNC coating concentration of 50 ppm (Fig. 9b), cracks appeared in the coating, likely due to tensile stresses induced during heat treatment. However, at a higher concentration of 150 ppm (Fig. 9c), the coating appears uniform and homogeneous,

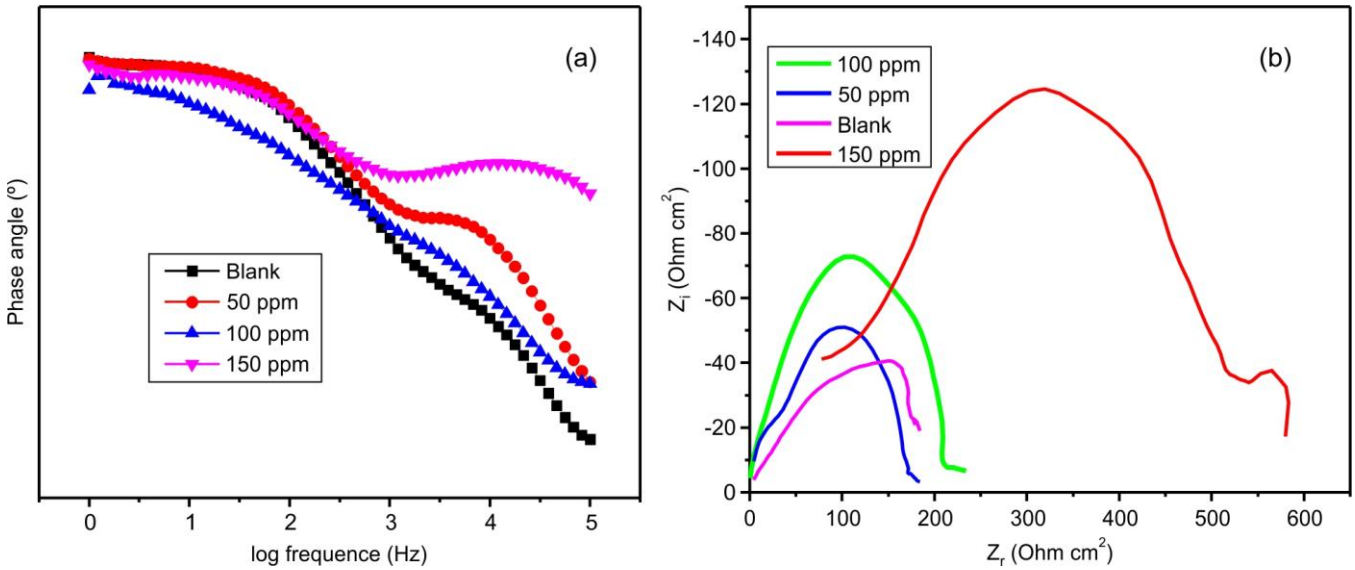

Fig. 8. Nyquist plot (a) bare and (b) epoxy coated mild steel in acidic condition

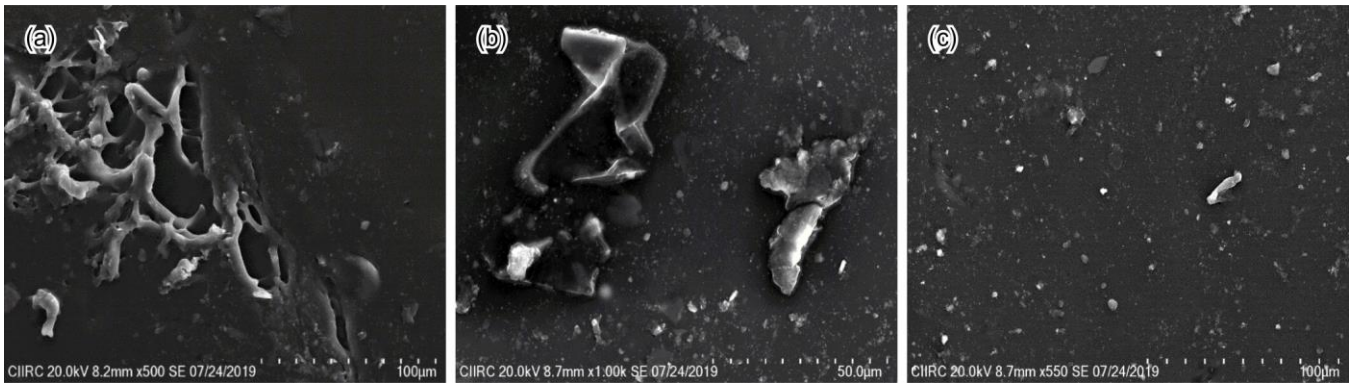

Fig. 9. SEM image of epoxy coated mild steel in acidic condition

effectively protecting the steel surface. These observations confirm that PGNC serves as an efficient corrosion inhibitor, with improved coating integrity at higher concentrations.

Conclusion

Inorganic coatings provide a strong bond between steel and polymer layers; however, their susceptibility to cracks and porosity limits their effectiveness. Incorporating inhibitors helps reduce these defects, enhancing the protective performance of coatings. In this study, nanocomposites of polyaniline and graphene (PGNC) were successfully synthesized *via in situ* polymerization. Comprehensive structural characterizations using XRD, TGA, SEM, FT-IR, Raman and UV-Vis techniques confirmed the formation and uniform distribution of PGNC within the polymer matrix. PGNC demonstrated excellent corrosion inhibition for mild steel in 0.25 M HCl solution, with corrosion rates decreasing as the inhibitor concentration increased. Thermogravimetric analysis showed that PGNC exhibits higher thermal stability than pure PANI, attributed to the deposition of PANI on the graphene matrix. XRD results revealed changes in the lattice structure due to PANI incorporation, while FT-IR and Raman spectra confirmed strong interactions between PANI and graphene. Electrochemical studies using potentiodynamic polarization demonstrated that epoxy coatings reinforced with PGNC provide significantly better corrosion resistance compared to epoxy alone. SEM analysis further confirmed the formation of uniform, crack-free coatings at various PGNC concentrations. Overall, these results highlight PGNC as an efficient corrosion inhibitor for mild steel in acidic environments.

ACKNOWLEDGEMENTS

The authors acknowledge the Principal and the management, RNS Institute of Technology, Bengaluru, India for the cooperation and for providing the necessary facilities.

CONFLICT OF INTEREST

The authors declare that there is no conflict of interests regarding the publication of this article.

REFERENCES

1. H. Wang, P. Shi, M. Rui, A. Zhu, R. Liu and C. Zhang, *Prog. Org. Coat.*, **139**, 105476 (2020); https://doi.org/10.1016/j.porgcoat.2019.105476.
2. N. Ruecha, R. Rangkupan, N. Rodthongkum and O. Chailapakul, *Biosensors and bio electronics*, **52** 13 (2014); https://doi.org/10.1016/j.bios.2013.08.018
3. L. Wang, X. Lu, S. Lei and Y. Song, *J. Mater. Chem. A*, **2**, 4491 (2014); https://doi.org/10.1039/C3TA13462H
4. S. Yang, S. Zhu and R. Hong, *Coatings*, **10**, 1215 (2020); https://doi.org/10.3390/coatings10121215
5. Z. Wu, X. Chen, S. Zhu, Z. Zhou, Y. Yao, W. Quan and B. Liu, *Sens. Actuators B Chem.*, **178**, 485 (2013); https://doi.org/10.1016/j.snb.2013.01.014
6. S. Dimitra and P.D. Praveen, *Chem. Paper*, **71**, 459 (2017). https://doi.org/10.1007/s11696-016-0044-0
7. S. Karthika, Jayadev and K. Raj, *Mater. Today Proc.*, **38(Part 5)**, 2493 (2021); https://doi.org/10.1016/j.matpr.2020.07.515
8. A.M. Solonaru and M. Grigoras, *Express Polym. Lett.*, **11**, 127 (2017); https://doi.org/10.3144/expresspolymlett.2017.14
9. B. Ramezanzadeh, G. Bahlakeh and M. Ramezanzadeh, *Corros. Sci.*, **137**, 111 (2018); https://doi.org/10.1016/j.corsci.2018.03.038
10. T.H. Han, N. Parveen, J.H. Shim, A.T.N. Nguyen, N. Mahato and M.H. Cho, *Ind. Eng. Chem. Res.*, **57**, 6705 (2018); https://doi.org/10.1021/acs.iecr.7b05314
11. K. Shetty, Jayadev, K. Raj and N. Mohan, *Mater. Today Proc.*, **27**, 2158 (2020); https://doi.org/10.1016/j.matpr.2019.09.087
12. W. Kai, L. Liwei, X. Wen, Z. Shengzhe, L. Yong, Z. Hongwei, and S. Zongqiang, *Int. J. Electrochem. Sci.*, **12**, 8306 (2017); https://doi.org/10.20964/2017.09.06
13. G.S. Hikku, K. Jeyasubramanian, A. Venugopal and R. Ghosh, *J. Alloys Compd.*, **716**, 259 (2017); https://doi.org/10.1016/j.jallcom.2017.04.324
14. P.A. Senthilvasan and M. Rangarajan, *Mater. Res. Express*, **5**, 045901 (2018); https://doi.org/10.1088/2053-1591/aace3f
15. P. Modak, S.B. Kondawar and D.V. Nandanwar, *Proc. Mater. Sci.*, **10**, 588 (2015); https://doi.org/10.1016/j.mspro.2015.06.010
16. A.S. Rao, B.S. Sannakashappanavar, A. Jayarama and R. Pinto, *Results Chem.*, **7**, 101533 (2024); https://doi.org/10.1016/j.rechem.2024.101533
17. N.J. Abdullah, A.F. Essa, and S.M. Hasan, *Iraqi J. Sci.*, **62**, 138 (2021); https://doi.org/10.24996/ijs.2021.62.1.13
18. N. Promphet, P. Rattanarat, O. Chailapakul, R. Rangkupan and N. Rodthongkum, *Sens. Actuators B Chem.*, **207**, 526 (2014); https://doi.org/10.1016/j.snb.2014.10.126
19. F. Xiao, S. Yang, Z. Zhang, H. Liu, J. Xiao, L. Wan, J. Luo, S. Wang and Y. Liu, *Sci. Rep.*, **5**, 9359 (2015); https://doi.org/10.1038/srep09359
20. Y. Sun, Q. Wang, C. Chen, X. Tan and X. Wang, *Environ. Sci. Technol.*, **46**, 6020 (2012); https://doi.org/10.1021/es300720f
21. V.V. Shunaev and O.E. Glukhova, *J. Phys. Chem. C*, **120**, 4145 (2016); https://doi.org/10.1021/acs.jpcc.5b12616
22. E.A. Sanches, J.C. Soares, R.M. Iost, V.S. Marangoni, G. Trovati, T. Batista, A.C. Mafud, A. Zucolotto and Y.P. Mascaren, *J. Nanomater.*, **2011**, 697071 (2011); https://doi.org/10.1155/2011/697071
23. Y. Du, P. Xiao, J. Yuan and J. Chen, *Coatings*, **10**, 892 (2020); https://doi.org/10.3390/coatings10090892
24. K. Zhang, L.L. Zhang, X.S. Zhao and J. Wu, *Chem. Mater.*, **22**, 1392 (2010); https://doi.org/10.1021/cm902876u
25. Z. Çıplak, A. Yıldız and N. Yıldız, *J. Energy Storage*, **32**, 101846 (2020); https://doi.org/10.1016/j.est.2020.101846
26. N. Mahato, N. Parveen and M.H. Cho, *Mater. Lett.*, **161**, 372 (2015); https://doi.org/10.1016/j.matlet.2015.08.138